ACS APPLIED MATERIALS & INTERFACES

Letter

www.acsami.org

Printing Stretchable Spiral Interconnects Using Reactive Ink Chemistries

Avinash Mamidanna, Zeming Song, Cheng Lv, Christopher S. Lefky, Hanqing Jiang, and Owen J. Hildreth*

School for the Engineering of Matter, Transport, and Energy, Arizona State University, Tempe, Arizona 85271, United States

Supporting Information

ABSTRACT: Stretchable electronics have important applications in health monitoring and integrated lab-on-a-chip devices. This paper discusses the performance of serpentine stretchable interconnects printed using self-reducing, silver reactive inks. It details process optimization, device fabrication, and device characterization, while demonstrating the potential applications for reactive inks and new design strategies in stretchable electronics. Devices were printed with an ethanol stabilized silver diamine reactive ink and cycled to stretch ratios of 140 and 160% over 1000 cycles with less than 2.5% variation in electrical resistance. Maximum deformation before failure was measured at 180% elongation. Additionally, interconnect deformation was compared to finite element analysis (FEA) simulations to show that FEA can be used to accurately model the deformation of low-strain printed interconnects. Overall, this paper demonstrates a simple and affordable route toward stretchable electrical interconnects.

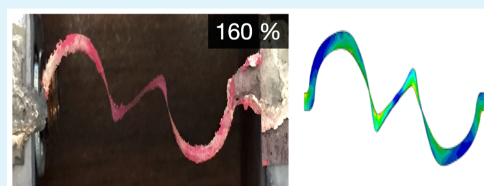

KEYWORDS: *stretchable electronics, drop-on-demand, printing, reactive inks, conductive inks, flexible electronics, serpentine*

Advances in conventional microelectronics go hand-in-hand with the exponential decrease in component size. As component sizes have decreased, new models for packaging have emerged with the microelectronics industry rapidly adopting System-on-a-Chip (SOC) approaches that combine multiple functionalities on a single chip.[1] For example, the processing chips in today's smart phones integrate CPU, GPU, and even motion processing onto a single die. However, some applications do not lend themselves to integration at the chip-level. For example, newer lab-on-chip biomedical sensors use discrete components to sense environment and transmit data.[2,3] Many of these devices require electronics spread across large areas with sensors at one location sending data to a processing unit in another location and then to an antennae circuit elsewhere. For "hard" devices, like our smart phones, this is not a problem; however, spanning large distances while maintaining electrical contact can be difficult for stretchable electronic devices.[1,4,5] These devices, ranging from integrated display panels[6,7] to health sensors,[8] require stretchable and deformable electrical interconnects between hard components to enable conformal devices.[9,10]

Connecting hard components through stretchable interconnects is a common approach for stretchable electronic design and fabrication. In this approach, high-quality functional devices are fabricated using traditional methods and then these "islands" are connected with a stretchable electrical interconnect. These stretchable interconnects can be fabricated using highly malleable/compliant electronic materials, such as low-temperature liquid metals,[11] or by designing the interconnect to mitigate local strain through out-of-plane deformation (e.g., buckled devices,[2,9] pop-up interconnects,[4,8] and serpentine-shaped interconnects[3,11−13]). Although flexible and stretchable interconnects are readily fabricated using conventional lithography techniques, integrating these hard components with the stretchable interconnect can be cumbersome due to the height difference between the component and the substrate. More importantly, interconnects fabricated using conventional lithography techniques are generally limited to metal thicknesses of ~1 μm, limiting the applicability of stretchable interconnects to low-current applications. Drop-on-Demand (DOD) printing of conductive inks could address these issues. This noncontact method can be used to connect devices with different heights using sacrificial support structures and the thicknesses on the order of tens of micrometers are readily printed with little effort.

This paper details a simple set of processes and chemistries to connect separate chips by printing free-standing stretchable interconnects based upon newer spiral designs.[4] Recent theoretical work comparing spiral interconnects to serpentine interconnects showed that that, for a given filling ratio and interconnect thickness, spiral interconnects are much more stretchable than spiral interconnects. To further demonstrate that spiral interconnects have low strains even for thick interconnects, DOD print was used to fabricate spiral interconnects spanning 10 mm and cycled 1000 times to stretch ratios of 160 and 180% with less than 2.5% variation in measured resistance. Additionally, finite element analysis (FEA) simulations of the deformed shape during stretching agree with optical images of actual samples, demonstrating that even though the printed interconnects are porous with nonuniform

Received: April 1, 2016
Accepted: May 9, 2016

 © XXXX American Chemical Society

cross-sections, the deformation can be accurately predicted even from simplified models. The printed stretchable interconnects can be used to connect many different type of functional units that are on isolated islands, such as CPU, memory, A/D converter, regulator, and bluetooth devices.

For this work, a low-temperature, self-reducing Ag ink was used as the basis to print high-quality silver interconnects.[14]

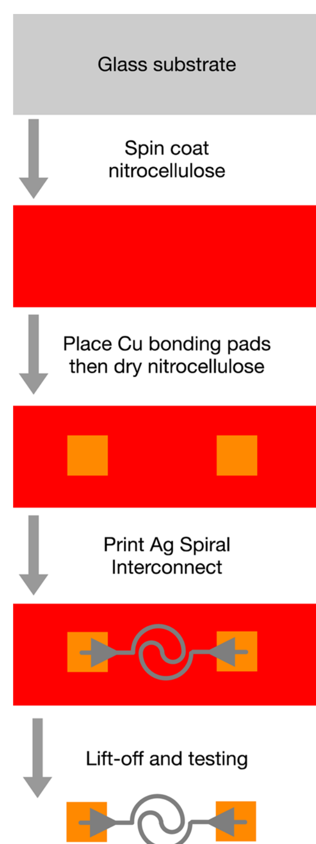

Figure 1. Schematic of stretchable interconnects fabrication process. A glass substrate is spin-coated with a uniform layer of nitrocellulose. Copper pads are placed in the nitrocellulose. The reactive silver ink spiral is then printed followed by lift-off in acetone then electrical and mechanical testing.

Unlike traditional particle-based inks that effectively print clusters of loosely connected particles, reactive inks print chemical reactions that, if properly designed, produce a high-quality material with excellent material properties at low temperatures. These reactive inks (also known as self-reducing or organometallic inks) are often easier to synthesize than nanoparticle inks and can be designed to react at temperatures lower than the sintering temperature of particle-based inks.[14−18] This paper details device fabrication, and device characterization while demonstrating the potential applications for reactive inks and new design strategies in stretchable interconnects. Overall, this paper demonstrates a simple and affordable route toward stretchable electrical interconnects.

The overall fabrication process is shown in Figure 1. Copper pads serving as a model "device" were fabricated by e-beam evaporation of 10/100 nm of Cr/Cu onto a 110 μm polyethylene substrate. Next, a layer of nitrocellulose was deposited onto a 25 mm × 50 mm glass slide using a VTC 100 vacuum spin coater. Two 30-s ramp steps were used from 500−2500 rpm increasing 2000 rpm/step. The copper-coated polymer pads were then peeled from the polyethylene carrier using tweezers and imbedded in nitrocellulose matrix approximately 10 mm apart with the top surface of the copper pad just barely above the nitrocellulose. This small distance reduced the thickness of the Ag ink needed to bridge the copper/nitrocellulose vertical gap. The substrate was left to dry at room temperature (∼27 °C) for 60−80 min.

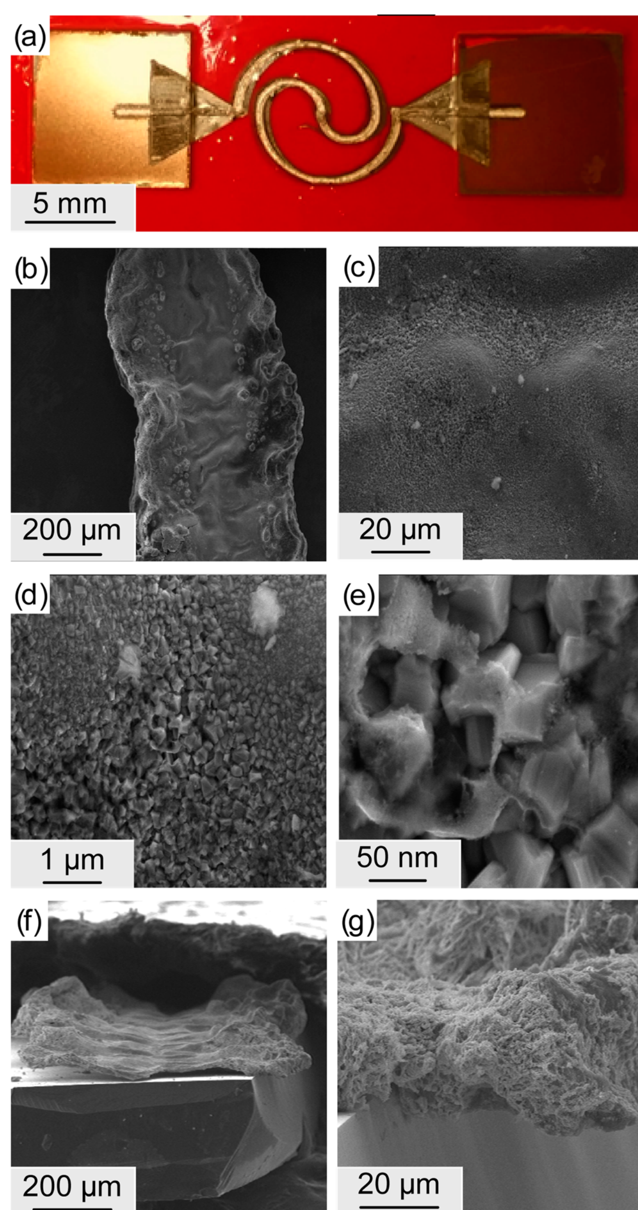

Figure 2. Drop-on-demand printed silver interconnect on the bilayer substrate before liftoff. (a) Triangular silver pads had been printed for enhancing the mechanical strength of the interface. 500 layers of the device were printed using 1:10 Ag:EtOH ink printed at 90 °C. (b−e) SEM micrographs showing that the silver is continuous across multiple length scales; (f, g) cross-section images showing that the printed line is 0.5−1 μm thick in the center and thickness to 20−30 μm on the edges.

To fabricate the stretchable interconnect, a slightly modified version of the Ag reactive ink detailed by Lewis' group[14] with the 2,3-butandiol humectant removed and the ink stabilized using ethanol. All chemicals were used as received. Two grams of silver acetate ($C_2H_3AgO_2$, anhydrous 99%, Alfa Aesar) was dissolved in 5.00 mL of 35 wt % ammonium hydroxide

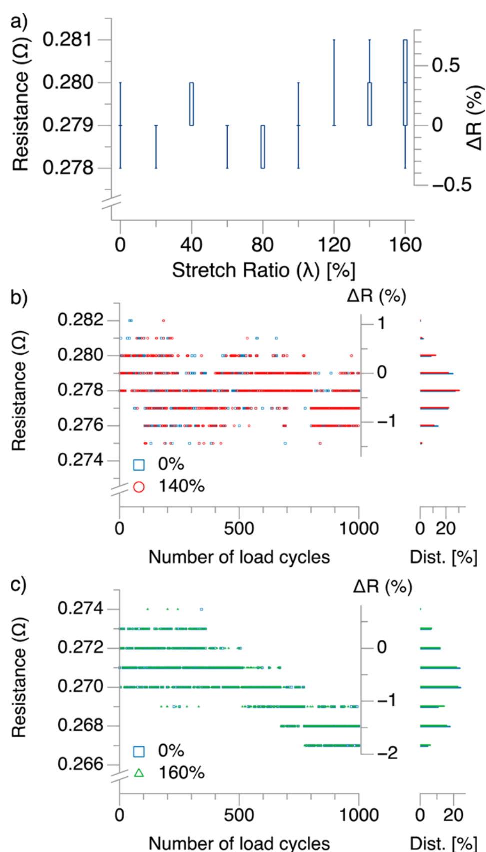

Figure 3. Graphs showing impact of elongation and cycles on the measured 2-point resistance across the spiral. (a) whisker plot of two-point resistance and ΔR(%) change measured between the copper pads at 20% increments in stretch ratio (λ). The total ΔR range was less than 1.2%. (b) The resistance at λ = 0 and 140% (blue square, red circle respectively) for 1000 stretch/relaxation cycles to 140% stretch ratio. Total variation in resistance is less than 2.5%. (c) The resistance at λ = 0 and 160% (blue square, green triangle, respectively) for 1000 stretch/relaxation cycles to 160% stretch ratio with a total variation in resistance of less than 2.5%.

(NH_4OH, ACS grade, BDH Chemicals). The solution was then stirred for 2 min on a vortex mixer. 0.40 mL of formic acid (CH_2O_2 − ACS reagent ≥96%, Sigma-Aldrich) was added in two steps and stirred at the end of each step. The ink was then allowed to sit for 12 h in the dark before being filtered through a 450 nm nylon filter and stored at 3 °C until use. For printing, the ink was removed from the refrigerator, allowed to warm to room temperature, and then diluted with ethanol (EtOH, Sigma-Aldrich) 10:1 EtOH:Ag ink by volume to reduce the thickness of each printed layer and create a more-dense silver structure.

Devices were printed using a Microfab Jetlab II Drop-on-Demand printing system with a 60 μm diameter MJ-ATP-01 piezoelectric nozzle. Print parameters (shown in Table S1) were optimized to minimize satellite droplet formation and the stage heated to 90 °C with a measured substrate temperature of 72 °C, and 7 mm × 7 mm squares were printed under identical conditions for electrical characterization using 4-point probe techniques. The spiral was printed with 500 passes of a 10:1 EtOH:Ag ink to ensure adequate mechanical strength during liftoff. Thirty layers of triangular pads are then printed with a 1:1 EtOH:Ag Ink at the interface between the copper bonding pads and the spiral to increase its robustness at this critical

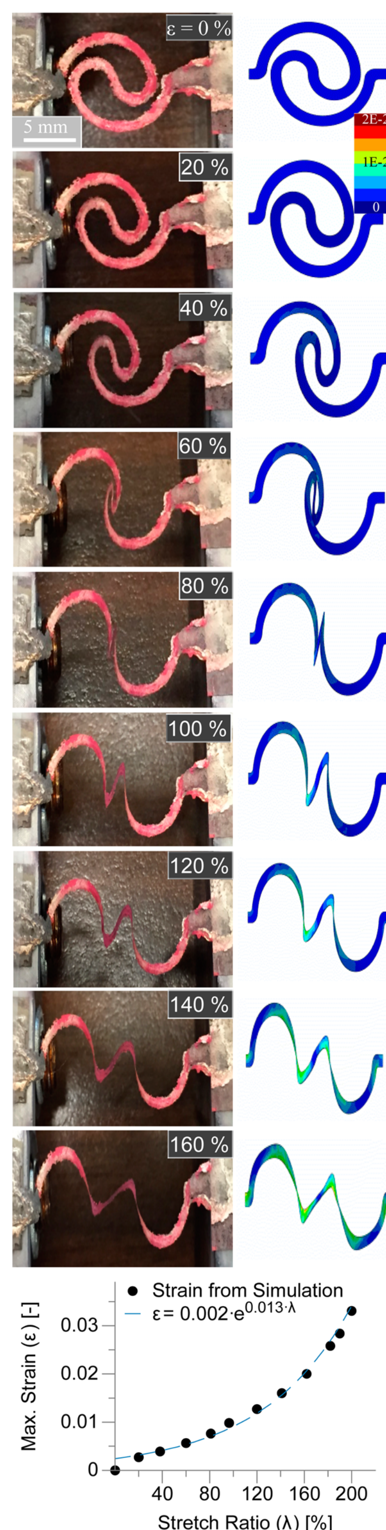

Figure 4. Comparison FEA vs experimental results for stretch ratios for λ = 0−160%. Notice that the simulation closely matches the shape of the experimental results. The graph at the bottom shows the maximum strain vs stretch ratio (λ) from the simulations. An exponential fit of $\epsilon = 0.002 \times e^{0.013\lambda}$ agrees well the simulated strain, showing that the strain starts extremely small and increases exponentially with stretch ratio.

interface. The printed device is then dipped in an acetone bath for 5−7 h to dissolve the nitrocellulose, leaving behind a free-

DOI: 10.1021/acsami.6b03922
ACS Appl. Mater. Interfaces XXXX, XXX, XXX−XXX

standing, stretchable interconnect between the two copper pads.

After printing, the silver interconnects were inspected using scanning electron microscopy (SEM) and energy-dispersive X-ray spectroscopy (EDS) to quantify physical morphology and elemental composition. From the optical image and SEM micrographs in Figure 2b−e, it is clear that the Ag structure is continuous across multiple length scales with some surface roughness and internal voids. The cross-section images in Figure 2d, e show that the printed interconnect is 0.5−1 μm thick in the center and thickness to 20−30 μm on the edges. The porous nature of the reactive silver ink makes the structure more susceptible capillary induced damage during the drying process and explains why, when less than 400 layers were used, the Ag interconnect would break apart during lift-off. Future work will detail methods to reduce the porosity of interconnects printed using Ag reactive ink; however, for this work, increasing the number of layers to 500 was sufficient to get a functioning interconnect that withstood the lift-off process.

EDS spectra of the Ag interconnects is shown in Figure S4 (with elemental composition summarized in Table S2) shows that the Ag lines are highly contaminated with carbon and oxygen content 26 and 14 at %, respectively. Despite the high levels of carbon and oxygen contamination, the resistance of the interconnect was reasonably low at 0.26−0.28 Ω over a line length of 50.4 mm.

To better characterize the electrical properties of the material, we printed and quantified 7 mm × 7 mm samples with 10 layers using a 4-point probe to get sheet resistance and cross-sectional SEM images for thickness. The sheet resistance was measured at 5.8 m$\Omega/\square$. The resistivity was calculated at 7.3 $\mu\Omega$ cm using $\rho = GtR_{\square}$; with $G = \frac{\pi}{\ln 2}\frac{b}{s}R_2\left(\frac{b}{s}, \frac{a}{b}\right)$;[19] the thickness, t, was measured at 3.4 μm using profilometry; the probe spacing, s, was 2 mm; the width and length (a, b) were both 7 mm. The geometry correction factor, R_2, was 0.80.[19]

The stretchability of the electrical interconnect was quantified by mounting the sample on a manually operated mechanical strainer with 0.5 mm gradations and measuring the 2-point electrical resistance with a digital multimeter (Agilent, 34461A). The elongation was cyclic from 0 to 140 or 160% and then back to 0% with a elongation/shortening rate of ∼16 mm/s (∼170%/s, cycle time ∼0.72 s). The graph in Figure 3a shows the resistance as a function of stretch ratio for one stretch cycle with a mean resistance of R_{single} = 0.279 Ω with total range in resistance, ΔR_{single} = 3 mΩ (1.2%) relative to the initial resistance. The graphs in Figure 3b, c show the range in resistance measurements as the device is cycled 1000 times between λ = 0:140% and λ = 0:160%, respectively. The ΔR% is shown on the right along with histogram showing the percentage distribution of the measured resistance values. The range in resistance variation was less than 2.5% for both tests of 1000 cycles. These results show that the spiral stretchable electrical interconnect has little to no degradation in electrical properties even after thousands of cycles at large stretch ratios. The λ = 140% test shows a nearly random distribution in resistance measurements while the λ = 160% test shows a slight decrease of 2mΩ (ΔR = 1%) over the last 500 cycles. The exact reason for the observed decrease is currently unknown and could possibly be attributed to changes in ambient environment. The stretch cycle tests were done slowly using manually driven linear stages over the course of 14 h for each test and the small, 2mΩ drift in resistance could be attributed to changes in ambient temperature and humidity. A second sample was fabricated and then stretched to failure to λ = 180%.

To better understand the deformation modes, finite element analysis (FEA) was carried out using a commercial FEA package (ABAQUS, Dassault Systemes, Waltham, MA, USA). Two types of calculation were used to study the buckling behavior of the spiral under given boundary conditions. eigenvalue analysis (i.e., prebuckling analysis) was used to calculate the modes of the model. After obtaining the mode shapes, the first mode shape is scaled and added to the undeformed geometry of the spiral as the imperfection. Then a general nonlinear static analysis (i.e., postbuckling analysis) was conducted to study the deformation behavior of the spiral upon loading. There are 1812 C3D8R elements (3D 8-node linear continuum elements with reduced integration) in the model. For this simulation, the thickness was set at 30 μm with a continuous width of 850 μm, the Young's modulus and Poisson's ratio of the silver electrode were assumed to be E = 83 GPa and ν = 0.37, respectively.[20] Figure 4 compares the optical images with the FEA models of the serpentine electrical interconnect from 0 to 160% elongation. The graph at the bottom of Figure 4 shows the maximum simulated strain vs stretch ratio from λ = 0% to λ = 200% at 20% increments (filled black circles). The simulated strain is fit as $\epsilon = 0.002 \times e^{0.013\lambda}$ (dashed line) with correlation value of 0.996, showing that strain starts extremely low and increase exponentially. Since the printed interconnect broke at λ = 180%, where the nominal strain predicted by the FEA simulations was only 0.02 (2%), well below the ultimate strain for polycrystalline silver but above the yield strain;[20] we can infer that the some portion of the stretchable interconnect yields without breaking if the magnitude of the stretch ratio is increased. Although the printed silver has a measured porosity of ∼80% and the model assumed 0% porosity, no major differences between the model and the experimental deflection were observed because of the low strain to stretch ratio of this spiral interconnect design. This is important because it confirms that simplified FEA models (continuous, isotropic material; uniform rectangular cross-section) can be used to predict the deformation shape of spiral interconnects under low strains even for porous interconnects with nonuniform cross sections. As a result, future printed stretchable interconnects can be optimized on computer prior to printing.

■ ASSOCIATED CONTENT

Supporting Information

The Supporting Information is available free of charge on the ACS Publications website at DOI: 10.1021/acsami.6b03922.

Details on the Microfab Jetlab II printer, nitrocellulose coating process, and RAW EDS spectra (PDF)

■ AUTHOR INFORMATION

Corresponding Author

*E-mail: owen.hildreth@asu.edu.

Author Contributions

The manuscript was written through contributions of all authors. All authors have given approval to the final version of the manuscript.

Notes

The authors declare no competing financial interest.

ACKNOWLEDGMENTS

Owen Hildreth acknowledges the support from Science Foundation of Arizona (Grant No. BSP 0615-15). Hanqing Jiang acknowledges the support from NSF (Grant No. CMMI-1462481).

REFERENCES

(1) Reuss, R. H.; Chalamala, B. R.; Moussessian, A.; Kane, M. G.; Kumar, A.; Zhang, D. C.; Rogers, J. A.; Hatalis, M.; Temple, D.; Moddel, G.; Eliasson, B. J.; Estes, M. J.; Kunze, J.; Handy, E. S.; Harmon, E. S.; Salzman, D. B.; Woodall, J. M.; Alam, M. A.; Murthy, J. Y.; Jacobsen, S. C.; Olivier, M.; Markus, D.; Campbell, P. M.; Snow, E. Macroelectronics: Perspectives on Technology and Applications. *Proc. IEEE* **2005**, *93*, 1239−1256.

(2) Kim, T. I.; McCall, J. G.; Jung, Y. H.; Huang, X.; Siuda, E. R.; Li, Y.; Song, J.; Song, Y. M.; Pao, H. A.; Kim, R. H.; Lu, C.; Lee, S. D.; Song, I. S.; Shin, G.; Al-Hasani, R.; Kim, S.; Tan, M. P.; Huang, Y.; Omenetto, F. G.; Rogers, J. A.; Bruchas, M. R. Injectable, Cellular-Scale Optoelectronics with Applications for Wireless Optogenetics. *Science* **2013**, *340*, 211−216.

(3) Webb, R. C.; Bonifas, A. P.; Behnaz, A.; Zhang, Y.; Yu, K. J.; Cheng, H.; Shi, M.; Bian, Z.; Liu, Z.; Kim, Y.-S.; Yeo, W.-H.; Park, J. S.; Song, J.; Li, Y.; Huang, Y.; Gorbach, A. M.; Rogers, J. A. Ultrathin Conformal Devices for Precise and Continuous Thermal Characterization of Human Skin. *Nat. Mater.* **2013**, *12*, 938−944.

(4) Lv, C.; Yu, H.; Jiang, H. Archimedean Spiral Design for Extremely Stretchable Interconnects. *Ext. Mech. Lett.* **2014**, *1*, 29−34.

(5) Yu, C.; Wang, Z.; Yu, H.; Jiang, H. A Stretchable Temperature Sensor Based on Elastically Buckled Thin Film Devices on Elastomeric Substrates. *Appl. Phys. Lett.* **2009**, *95*, 141912.

(6) Gazotti, W. A.; Casalbore Miceli, G.; Geri, A.; Berlin, A.; de Paoli, M. A. An All-Plastic and Flexible Electrochromic Device Based on Elastomeric Blends. *Adv. Mater.* **1998**, *10*, 1522−1525.

(7) Moonen, P. F.; Yakimets, I.; Huskens, J. Fabrication of Transistors on Flexible Substrates: from Mass-Printing to High-Resolution Alternative Lithography Strategies. *Adv. Mater.* **2012**, *24*, 5526−5541.

(8) Thomas, M. S.; Millare, B.; Clift, J. M.; Bao, D.; Hong, C.; Vullev, V. I. Print-and-Peel Fabrication for Microfluidics: What's in it for Biomedical Applications? *Ann. Biomed. Eng.* **2010**, *38*, 21−32.

(9) Schwartz, G.; Tee, B. C. K.; Mei, J.; Appleton, A. L.; Kim, D. H.; Wang, H.; Bao, Z. Flexible Polymer Transistors with High Pressure Sensitivity For Application in Electronic Skin and Health Monitoring. *Nat. Commun.* **2013**, *4*, 1859.

(10) Zang, Y.; Zhang, F.; Di, C.-A.; Zhu, D. Advances of Flexible Pressure Sensors Toward Artificial Intelligence and Health Care Applications. *Mater. Horiz.* **2015**, *2*, 140−156.

(11) Kim, H.-J.; Son, C.; Ziaie, B. A Multiaxial Stretchable Interconnect using Liquid-Alloy-Filled Elastomeric Microchannels. *Appl. Phys. Lett.* **2008**, *92*, 011904.

(12) Sosin, S.; Zoumpoulidis, T.; Bartek, M.; Wang, L.; Dekker, R.; Jansen, K. M. B.; Ernst, L. J. Free-Standing, Parylene-Sealed Copper Interconnect for Stretchable Silicon Electronics. *Proc. - Electron. Compon. Technol. Conf.* **2008**, 1339−1345.

(13) Jablonski, M.; Lucchini, R.; Bossuyt, F.; Vervust, T.; Vanfleteren, J.; De Vries, J. W. C.; Vena, P.; Gonzalez, M. Impact of Geometry on Stretchable Meandered Interconnect Uniaxial Tensile Extension Fatigue Reliability. *Microelectron. Reliab.* **2015**, *55*, 143−154.

(14) Walker, S. B.; Lewis, J. A. Reactive Silver Inks for Patterning High-Conductivity Features at Mild Temperatures. *J. Am. Chem. Soc.* **2012**, *134*, 1419−1421.

(15) Lee, H. M.; Lee, H. B.; Jung, D. S.; Yun, J.-Y.; Ko, S. H.; Park, S. B. Solution Processed Aluminum Paper for Flexible Electronics. *Langmuir* **2012**, *28*, 13127−13135.

(16) Lee, H. M.; Seo, J. Y.; Jung, A.; Choi, S.-Y.; Ko, S. H.; Jo, J.; Park, S. B.; Park, D. Long-Term Sustainable Aluminum Precursor Solution for Highly Conductive Thin Films on Rigid and Flexible Substrates. *ACS Appl. Mater. Interfaces* **2014**, 15480−15487.

(17) Farraj, Y.; Grouchko, M.; Magdassi, S. Self-Reduction of a Copper Complex MOD Ink for Inkjet Printing Conductive Patterns on Plastics. *Chem. Commun.* **2015**, *51*, 1587−1590.

(18) Rosen, Y.; Grouchko, M.; Magdassi, S. Printing a Self-Reducing Copper Precursor on 2D and 3D Objects to Yield Copper Patterns with 50% Copper's Bulk Conductivity. *Adv. Mater. Interfaces* **2015**, *2*, 1400448.

(19) Smits, F. M. Measurement of Sheet Resistivities with the Four-Point Probe. *Bell Syst. Tech. J.* **1958**, *37*, 711−718.

(20) Cardarelli, F. *Materials Handbook*; Springer−Verlag: London, 2008; Chapter 3, pp 194−195.

DOI: 10.1021/acsami.6b03922
ACS Appl. Mater. Interfaces XXXX, XXX, XXX−XXX